GEOCHEMISTRY

The role of continental subduction in mantle metasomatism and carbon recycling revealed by melt inclusions in UHP eclogites

Alessia Borghini[1]*, Gautier Nicoli[1], Silvio Ferrero[2,3], Patrick J. O'Brien[1], Oscar Laurent[4,5], Laurent Remusat[6], Giulio Borghini[7], Sula Milani[7]

Copyright © 2023 The Authors, some rights reserved; exclusive licensee American Association for the Advancement of Science. No claim to original U.S. Government Works. Distributed under a Creative Commons Attribution NonCommercial License 4.0 (CC BY-NC).

Subduction is the main process that recycles surface material into the mantle. Fluids and melts derived by dehydration and partial melting reactions of subducted continental crust, a major reservoir of volatiles (i.e., H_2O and CO_2) and incompatible elements, can substantially metasomatize and refertilize the mantle. Here, we investigate glassy inclusions of silicate melt of continental origin found in Variscan ultrahigh-pressure eclogites to assess the continental crust contribution to mantle metasomatism and the journey of volatiles, carbon in particular, to the deep roots of mountain belts. We argue that the melt preserved in these inclusions is the agent responsible for mantle metasomatism and subsequent ultrapotassic magmatism in the Variscides. We propose that continental subduction can redistribute a substantial volume of carbon in the continental lithosphere, which is subsequently transferred to the continental crust during postcollisional magmatism and stored for a time length longer than that of the modern carbon cycle.

INTRODUCTION

Fluids and melts generated by devolatilization and partial melting of buried surface materials in subduction zones are responsible for metasomatism of the overlying mantle wedge (*1*–*3*), thus playing a major role in controlling element fractionation associated with crustal differentiation in Earth's lithosphere (*4*, *5*). In convergent settings, fluids and melts can be released at depth by both oceanic lithosphere and continental crust. In the case of the oceanic lithosphere, the components released during devolatilization and partial melting reactions, after being temporarily stored in the mantle wedge, may return to Earth's surface as the magmatic and volatile products of volcanic arc activity (*1*, *2*, *6*). Additional evidence for this mantle-crust interaction is found in the overriding plate in the form of ultrapotassic plutons emplaced in the latter stage of continental collision (*7*–*9*), a common occurrence in both modern arc settings (*10*) and eroded collisional belts. However, studies on the quantification of remobilization of surface material and transfer of volatiles, notably carbon, to the mantle have so far mainly focused on the oceanic lithosphere [(*11*) and references therein], thus leaving the impact of continental subduction on the global carbon budget of the deep Earth poorly constrained (*12*). In this work, we show that volatiles and incompatible elements derived from the felsic continental crust substantially contribute to mantle enrichment and carbon storage in the deep crust, upper mantle, and postcollisional (ultra-)potassic rocks.

Exhumed (ultra)high-pressure [(U)HP] rocks provide a direct window into deep lithospheric processes (*9*). Analogous to peritectic minerals in crustal migmatites (*13*), eclogitic garnets can also trap primary melt and fluid inclusions from metasomatic agents present at (U)HP metamorphic conditions (*14*, *15*). The melt enclosed in primary inclusions during high-grade (U)HP metamorphism does not experience CO_2 degassing before entrapment (*11*, *16*), unlike melt in inclusions from low-pressure arc basaltic magmas, as CO_2 solubility in silicate melts strongly increases with pressure (*17*). Moreover, previous in situ measurements have shown that preserved melt inclusions in metamorphic rocks have maintained their original H_2O content (*18*–*20*). Thus, (U)HP inclusions represent a powerful tool to investigate mobilization of volatiles associated with the subduction of the continental crust (*13*, *21*). We targeted UHP eclogites embedded in diamond-bearing granulitic gneisses (*22*, *23*) from the Saidenbach Reservoir in the Erzgebirge, Bohemian Massif (Germany). These eclogites experienced peak metamorphism likely at the same conditions of the surrounding gneisses, 1000°C and 4.5 GPa (*24*). The former, originally mafic dykes, were subducted along with continental felsic material and subsequently involved in the continent-continent collision responsible for the formation of the Variscan orogenic belt in Europe (*25*). These eclogites contain preserved primary melt inclusions, some of them glassy, trapped in garnet. Their characterization provides quantitative data on the nature and budget of crustal-derived volatiles and incompatible elements at 130 to 150 km depth.

Building mountain ranges is a complex process that balances consumption and production of carbon (*25*, *26*). The study of the deep melts, the medium in which volatiles are preferentially partitioned at high P and T, trapped in inclusions is possibly the most fruitful approach for shedding light not only on the past but also on the future evolution of modern orogens. In many respects, the Bohemian Massif could be regarded as representative of what will become of the present-day Himalaya-Tibet-Karakoram-Pamir system (*25*).

[1]Institute of Geosciences, University of Potsdam, 14476 Potsdam, Germany. [2]Dipartimento di scienze Chimiche e Geologiche, University of Cagliari, 09042 Monserrato, Italy. [3]Museum für Naturkunde (MfN), Leibniz-Institut für Evolutions- und Biodiversitätsforschung, 10115 Berlin, Germany. [4]ETH Zürich, Institute for Geochemistry and Petrology, 8092 Zürich, Switzerland. [5]CNRS, Géosciences Environnement Toulouse, Observatoire Midi-Pyrénées, 31400 Toulouse, France. [6]Museum National d'Histoire Naturelle, 75005 Paris, France. [7]Dipartimento di Scienze della Terra "Ardito Desio", University of Milano, 20133 Milano, Italy.
*Corresponding author. Email: borghini@uni-potsdam.de

RESULTS

Melt inclusions in UHP eclogites of Saidenbach

The Saidenbach UHP eclogites are dominated by garnet, clinopyroxene, and minor quartz (Fig. 1A and table S1). The garnet shows a core with composition $Prp_{28}Alm_{44}Grs_{27}Sps_1$ [Mg# = 40 where Mg# = molar $Mg/(Mg + Fe^{2+}_{tot}) \times 100$] and a narrow rim slightly higher in Alm and lower in Grs. The clinopyroxene has an average jadeite (Jd) content of 44 mol % (Mg# = 77). The inner part of garnet contains primary melt inclusions, both glassy and polycrystalline (i.e., nanogranitoids) (*27*), arranged as clusters (Fig. 1). Polycrystalline quartz pseudomorphing former coesite is also present in the same microstructural position (Fig. 1B) (*28*). The coexistence of coesite and melt inclusions in the same cluster indicates that the melt was trapped at UHP metamorphic conditions, thus likely at the metamorphic peak.

The glassy inclusions, 2 to 4 μm in diameter, represent <10% of the clusters, often exhibit a shrinkage bubble (Fig. 1D), and are hydrous, as shown by the Raman spectrum (Fig. 1F). Nanogranitoids are generally bigger, 5 to 20 μm in diameter, and contain a constant mineral assemblage of kumdykolite (orthorhombic polymorph of $NaAlSi_3O_8$), quartz, kokchetavite (hexagonal polymorph of $KAlSi_3O_8$), biotite, white mica, calcite, and rare graphite (Fig. 1, C

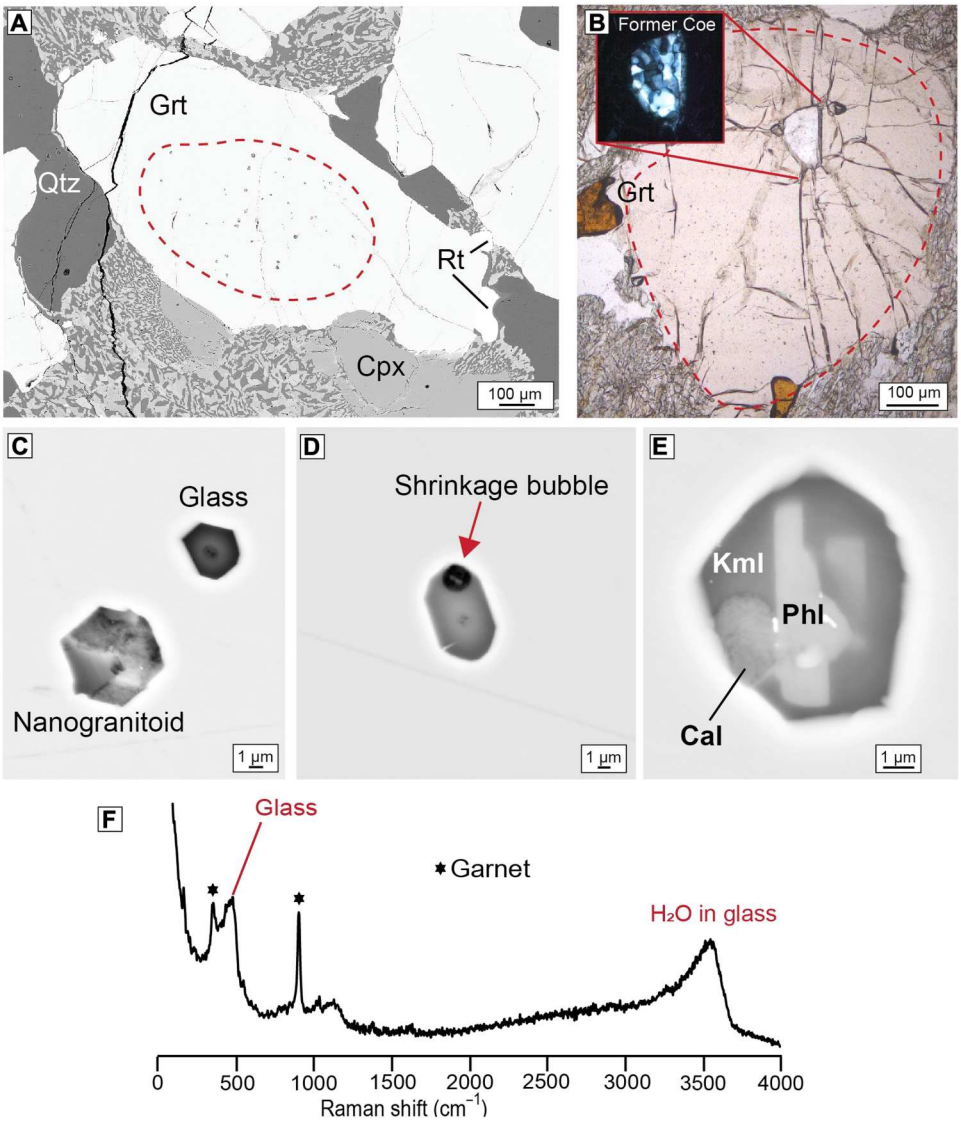

Fig. 1. UHP eclogites of Saidenbach, Erzgebirge, Germany. Backscattered electron (BSE) image (A) and photomicrograph (B) of eclogite texture and BSE images of melt inclusions (C to E). (**A**) Eclogite dominated by garnet (Grt) and clinopyroxene (Cpx) with minor quartz (Qtz) and accessory coarse-grained rutile (Rt). Grt contains a cluster of melt inclusions (dashed red line). (**B**) Detail of Grt with inclusion of polycrystalline quartz (in the red box inclusions in cross-polars) surrounded by radial cracks and interpreted as former coesite (Coe), in the same microstructural position with the cluster of melt inclusions (dashed red line). Melt inclusions are randomly distributed; they are both glassy (**C** and **D**) and crystallized as nanogranitoids (C to E). Some glassy inclusions contain a shrinkage bubble (red arrow) (D). The darker spots visible in the middle of the glassy inclusions are beam damages due to analysis. (**E**) Nanogranitoids are bigger than glassy inclusions; they have a regular shape that mimics that of the host mineral (i.e., negative crystal), and they consist of kumdykolite (Kml), phlogopite (Phl), calcite (Cal), kokchetavite, and quartz. (**F**) Raman spectrum of a preserved glassy inclusion in which the OH bands are visible.

and E), consistent with crystallization from a crustal-derived anatectic melt (*29*). The presence of feldspar polymorphs indicates that nanogranitoids are chemically preserved as the reopening of the system, through cracking or decrepitation, would have caused them to convert to their more stable counterparts (*30*). Despite behaving differently on cooling, glassy inclusions and nanogranitoids occur in the same cluster and thus contain the same melt (*27*, *31*), as confirmed by microchemical analyses (Fig. 2). Nanogranitoids were successfully rehomogenized in the multianvil apparatus at 1000°C and 4.5 GPa, the minimum conditions expected for the formation of the garnet in the Erzgebirge UHP unit (*24*), and thus likely to correspond to the entrapment conditions of the melt. The attained rehomogenization confirms that garnet and melt were both stable at the metamorphic peak conditions as demonstrated in previous studies (*19*, *27*, *29*). Preserved and rehomogenized glassy inclusions are granitic in composition, rich in alkalis [$Na_2O + K_2O = 9.31$ weight % (wt %) and $Na_2O/K_2O = 0.75$], and slightly peraluminous [alumina saturation index: molar $Al_2O_3/(Na_2O + K_2O + CaO) = 1.10$] and have a low magnesium number (Mg# = 27; see table S2). The melt trace element signature shows features in agreement with a continental crust origin, such as enrichment in large ion lithophile elements (LILEs; in particular Cs), Th, U, Pb, Li, B, and light rare earth elements (LREEs) and depletion of Nb and Ti (Fig. 3 and table S4) (*32*). The application of LREE thermometry based on experiments on the solubility of monazite in granitic melt (*33*) suggests temperatures of melt entrapment ranging between 610° and 950°C with an average at 725°C (see Materials and Methods).

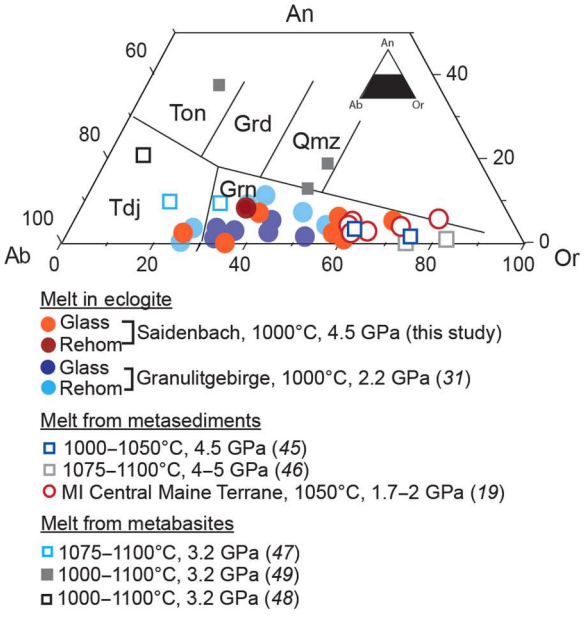

Fig. 2. Major element composition of Saidenbach eclogites melt inclusions. Normative anorthite-orthoclase-albite (An-Or-Ab) diagram where the melt from Saidenbach samples, measured on both glassy (Glass) and rehomogenized (Rehom) inclusions (this study), are compared with data from literature. Circles are used for natural melts, squares for experiments: Granulitgebirge eclogites (*31*); melts from partial melting of metasediments at UHP conditions (*45*, *46*); melts from rehomogenized nanogranitoids in metasediments of the Central Maine Terrane (*19*), Connecticut, USA; and melts from HP—UHP partial melting of metabasites (*47*–*49*). Compositional fields in the diagram are from (*92*). For details on melt composition and experimental conditions, see tables S2 and S3.

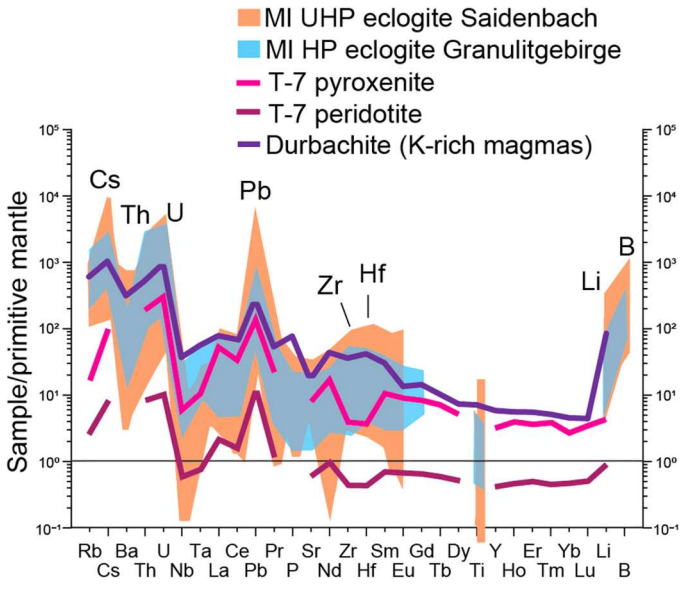

Fig. 3. Trace element patterns of melt inclusions and bulk rock. Primitive mantle-normalized (*93*) [except for B (*94*)] patterns of the melt inclusions in garnets of the UHP eclogites of Saidenbach (see table S4) compared with melt inclusions in HP eclogites of the Granulitgebirge (*3*, *31*) and the bulk rock compositions of metasomatized mantle rocks (peridotites and pyroxenites) of the T-7 borehole (*52*) and the average bulk rock values for the durbachite suite (*54*).

These temperatures are substantially lower than those inferred for entrapment (1000°C) based on complete experimental rehomogenization of the inclusions as well as the peak equilibration of the diamond-bearing metasediments [1000°C (*24*)] and for the UHP ultramafic rocks in the same metamorphic unit [i.e., the gneiss-eclogite unit (*34*). The successful rehomogenization of the inclusions, the compositional match between the preserved glassy inclusions and the rehomogenized ones, and the general agreement on the peak T of the unit suggest that 1000°C rather than 725°C is more likely to represent the minimum T of entrapment. Moreover, using a different solubility model [i.e., Zr calibrated for high pressures; (*35*)], we obtain temperatures of 1040°C that overall support our hypothesis for melt entrapment at minimum 1000°C, indicating that the discrepancy observed for LREE-solubility thermometry may result from complexities in the accessory mineral saturation processes upon the production and evolution of the Saidenbach melts.

The H_2O content of the inclusions ranges between 3.14 and 5.23 wt % (Fig. 4A). The measured CO_2 content of inclusions ranges between ~600 and 28,880 parts per million (ppm) (Fig. 4A, fig. S1, and table S5), with the rehomogenized inclusion containing more CO_2 (28,880 ppm) than the preserved glassy inclusions (2470 ppm in average). This is entirely expected, as CO_2 exsolves from the trapped melt on cooling and depressurization (*36*) and is sequestered in the shrinkage bubble visible in the glassy inclusions (Fig. 1D). Rehomogenization experiments on unopened inclusions still enclosed in the garnet led instead to the redissolution of the CO_2 into the melt, thus allowing the retrieval of the original CO_2 content of the melt at depth (*36*). Our measurements on the preserved glassy inclusions were corrected using a mass balance approach by integrating the amount of CO_2 originally

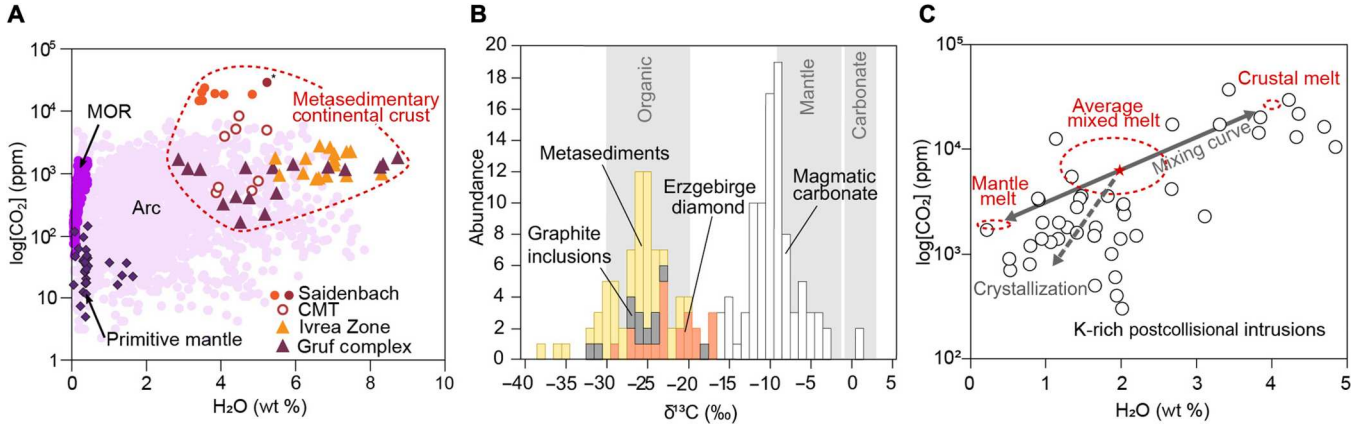

Fig. 4. Volatiles content in melt inclusions. (**A**) H_2O (wt %) and CO_2 (ppm) content of glass and a rehomogenized (indicated with an asterisk) nanogranitoid from Saidenbach eclogites measured and corrected by NanoSIMS (error bar smaller than the symbol) and compared with H_2O and CO_2 contents of lower continental crust melt inclusions in granulites [Central Maine Terrane (CMT) (*19*), Ivrea Zone (*20*), and Gruf Complex (*61*)]. See table S5 for volatiles data, and for NanoSIMS calibration curves, see fig. S1. Primitive mantle, mid-oceanic ridges (MOR), and arc volcanoes after (*13*). The dashed area indicates the compositions of melt derived from the metasedimentary continental crust. (**B**) Carbon isotopic compositions in the Erzgebirge [see table S6 for $\delta^{13}C$ data of carbonate (*76*), calcite (*75*, *77*, *95*), and dolomite (*77*) of postcollisional mineralization and of diamond in garnet (*66*), whole rock (*68*), and graphite in zircon (*65*) of metasediments of the Erzgebirge]. Shaded areas for the range of organic and carbonate $\delta^{13}C$ values after (*70*). The mantle values are from (*71*). (**C**) CO_2 and H_2O content of mantle and crustal melt mixing compared with potassium-rich postcollisional intrusions in the Bohemian Massif (empty circles) (*96*–*99*). See table S7 for CO_2 and H_2O data of (ultra)potassic magmatic rocks. The star indicates the average composition of the calculated melt. The dashed arrow indicates the inferred general decrease in melt CO_2 and H_2O concentration during ascent and cooling due to the increase in melt/fluid immiscibility and the partition of volatile species between these two phases.

present in the vapor bubble (see Materials and Methods). It results in a total amount of CO_2 held in glassy inclusions (melt + vapor) of 20,180 ± 4440 ppm, close to what we measured in the rehomogenized inclusion.

DISCUSSION

Saidenbach melt inclusions compared with multiphase solid inclusions in UHP rocks

The occurrence of polyphase inclusions in garnet is a rather common feature of UHP eclogites (*14*, *37*–*43*). They are generally identified as multiphase solid inclusions (MSIs) and interpreted either as melt inclusions (*37*–*41*) or as remnants of supercritical silicate-rich aqueous fluid inclusions (*14*, *42*, *43*). MSIs were identified mainly in the UHP eclogites in the Dabie Mountains (*37*–*39*, *41*), in the zoisite-bearing UHP eclogites of the Sulu Orogen in China (*40*), and the Kokchetav complex (Kazakhstan) (*44*). The MSIs in the Dabie and Sulu differ substantially in terms of microstructure, mineral assemblage, presence of glass, and compositions from the melt inclusions in Saidenbach samples. The former contain indeed variable amounts of K-feldspar + quartz ± plagioclase ± barite ± zoisite/epidote ± carbonates ± zircon (*37*–*41*) and were interpreted as evidence of partial melting of mafic eclogites under UHP conditions (*37*–*40*). In general, such inclusions are not pristine as they show clear evidence of postentrapment decrepitation, e.g., irregular shape, protrusion textures, radial cracks surrounding the inclusions, and the presence of a network of thin healed cracks in the host mineral (*39*–*41*). Decrepitation leads to OH loss, which, in turn, may explain the absence of OH-bearing phases in such MSIs, unlike nanogranitoids (*27*). In terms of trace elements, the Dabie and Sulu MSIs display a dominant Ba-positive anomaly, along with positive anomalies of Pb, U, Li, and Sr and negative anomalies of Th, Zr, and Hf. To explain such features, these inclusions were previously interpreted as the result of a reaction between an enclosed mineral, e.g., coesite and rutile, and an external fluid infiltrating the garnet during the first stage of exhumation at HP (*41*).

In comparison, the melt inclusions at Saidenbach range from glassy to polycrystalline in the same cluster, the mineral assemblage is constantly granitic, and they have a negative crystal shape without any decrepitation crack, even healed ones, connecting to the host boundary. From the geochemical point of view, the melt inclusions investigated here display a dominant positive anomaly in Cs, Th, U, and Pb and a slight enrichment in Zr and Hf, whereas Ba is only present in low concentrations (Fig. 3). All of these features, coupled with the successful rehomogenization of the nanogranitoids (*27*, *29*) and the presence of glass with limited H_2O concentrations, indicate that these inclusions were former melt droplets trapped during garnet growth, rather than remnants of supercritical silicate-rich aqueous fluid. Hence, Saidenbach melt inclusions represent a snapshot of processes happening at (near) peak metamorphic conditions rather than along the retrograde path.

The MSIs in the Kokchetav complex are of two types, type M and type L, found in melanosomes and leucosomes, respectively. Type M inclusions are concentrated in the central part of the garnets forming irregular clusters and they have been interpreted to have formed at peak conditions: For this reason, they will be the only type considered here for comparison. These inclusions contain a wide variety of rock-forming minerals and accessory phases, particularly quartz, biotite, phengite, kyanite, plagioclase, K-feldspar, Ba-feldspar, chlorite and rutile, ilmenite, apatite, zircon, baddeleyite, allanite, monazite, REE-carbonates, and sulfides. Inclusion size is extremely variable from 1 μm to over 1 mm, with the bigger inclusions often surrounded by radiating cracks. Melt composition obtained via rehomogenization of type M inclusions is granitic with high concentration of LREE, Th, U, Pb, and LILE, consistent with a continental crustal origin. Once again, the melt inclusions of

Saidenbach differ substantially in terms of both microstructural features, i.e., they have a rather constant size (2 to 20 μm) and no decrepitation cracks, and phase assemblage: They contain a much more restricted number of phases (only quartz, feldspar polymorphs, micas, and calcite). Similarities are found instead in their geochemistry, as the two melts show similar major and trace elements, a feature that supports the continental crust origin of the melt trapped in Saidenbach eclogites.

Anatectic melt as metasomatic agent and element redistribution during subduction

As a general rule, melts with similar signatures are likely to have similar sources and share a similar genetic process (*3*). In the case of the Saidenbach eclogites, the most likely origin is external, i.e., metasomatic, as already proposed for melts trapped in HP eclogites from the nearby Granulitgebirge (*3*), which indeed show similar compositions for both major and trace elements (Figs. 2 and 3). Melt in Saidenbach eclogites is more akin to anatectic melts from silicic continental crust rather than from mafic protoliths (Fig. 2), as shown by the comparison with both natural and experimental HP (*19*) and UHP melts from metasediments (*45*, *46*) and metabasites (Fig. 2 and table S3) (*47*–*49*). This signature is consistent with the involvement of phengite in the melt-producing reaction (*3*), pointing to the surrounding phengite-bearing metasedimentary rocks—some also microdiamond bearing (*24*)—as a possible source.

An internal production of the melt can be instead ruled out. Melting of mafic rocks in UHP experiments mainly produces a tonalitic-trondhjemitic-granodioritic melt rather than a granitic melt (Fig. 2). However, experiments also show that the first melt fraction (5 to 10 volume %) can have a granitic composition (*47*, *49*, *50*), but with the progression of the reaction, K-rich phases are completely consumed and clinopyroxene breaks down, driving the melt toward a more tonalitic composition (Fig. 2) (*51*). The microstructures observed in the rocks are inconsistent with this hypothesis. According to experiments, eclogite melting would produce a small amount of melt coexisting with a large portion of solids (as residue) (*49*), including a second generation of garnet capable of trapping melt as inclusions. However, neither residue nor two different generations of garnet can be identified in Saidenbach eclogites. Thus, the most likely scenario to explain the presence of melt inclusions in the garnets of Saidenbach eclogites is a metasomatic interaction between a melt generated in the continental crust at metamorphic peak conditions and former intrusive mafic layers (e.g., dykes), already present in the continental package [see discussion in (*3*)]. This melt-rock interaction originated the eclogites studied in this contribution.

The anatectic melt displays a trace element pattern close to that of metasomatized mantle rocks in multiple locations of the Bohemian Massif [e.g., T-7 borehole (*3*, *52*) and Horní Bory (*53*), respectively, in the northwest (NW) and east-southeast (ESE) portions] (Fig. 3). Such a pattern also has notable similarities with postcollisional ultrapotassic plutonic rocks, e.g., durbachite series, vaugnerites, appinites, shoshonites, and some lamprophyres through the geological record (*3*, *8*, *54*–*56*) (Fig. 3). These potassic intrusions show a peculiar composite signature with enrichments in compatible elements (Cr, Ni, and high Mg#) and incompatible ones (LILE, LREE, U, and Th). The former indicates a mantle origin whereas the latter points toward a crustal origin. This contradictory signature is explained with the formation of the (ultra)potassic magmas via partial melting of a mantle previously metasomatized by a mature crustal component (*8*, *54*, *57*, *58*), similar to the melt trapped in both Saidenbach eclogites (this study) and HP eclogites of the Granulitgebirge (*3*, *31*). Together, these similarities suggest that mantle metasomatism through partial melting of a deeply subducted continental material is widespread beneath the Bohemian Massif. Given the wide distribution of (ultra)potassic postcollisional rocks worldwide (*8*, *55*), it is also possible that this process is more common in collisional orogens than previously expected (*9*, *41* and references therein, *52*). Hence, we argue that the melt preserved in these UHP eclogites represents the first natural example of ultradeep crustal melt and pristine metasomatic agent capable of refertilizing the overlying mantle wedge in the context of continental subduction.

Consequences for carbon and water recycling

One of the main strengths of melt inclusions in metamorphic rocks is the fact that they record the volatile content of the melt at the moment of entrapment (*13*, *18*), hence providing an opportunity to investigate the redistribution of volatile elements from the surface to the mantle. In Saidenbach eclogites, the H_2O content of the melt (3.89 wt % in average; see table S5) is within error very similar to the one measured in other melts produced by the partial melting of metasediments in continent collision settings (~5 to 6 wt %, see table S5) (Fig. 4A). One caveat worth pointing out is related to what these H_2O values measured in glassy inclusions actually represent. Recently, it was shown how glassy inclusions in natural migmatites have generally a lower amount of H_2O with respect to the crystallized ones (nanogranitoids) present in the same cluster (*60*). The dataset presented in this contribution shows that preserved glassy inclusions contain ~4 wt % of H_2O on average, ~1 wt % less than the amount measured in the rehomogenized one, a former nanogranitoid, hence expected to be richer in water. It thus appears possible that H_2O contents may be slightly underestimated, around 20% relative based on the ratio between H_2O content in glassy and rehomogenized inclusions, when only glassy inclusions are considered to obtain data on the volatiles in the melt, in agreement with the available previous work on melt inclusions in metamorphic rocks (*59*).

The CO_2 concentration in the melt is high, ca. 16,000 to 29,000 ppm, and is overall substantially greater than the average content in melt inclusions from lower pressure metasediments (ca. 200 to 2400 ppm) (*20*, *61*) and HP granulites (ca. 500 to 8000 ppm) (*19*) (Fig. 4A), arguing for an increase in crustal carbon content with depth (Fig. 4A). Such a high CO_2 content in the melt is not unexpected in UHP rocks, as the solubility of CO_2 in (anhydrous) melts is directly proportional to the pressure (*17*). The solubility of CO_2 in rhyolitic melts is ca. 5700 ppm CO_2/GPa (*17*), suggesting a CO_2 content in the melt of ~25,700 ppm at 4.5 GPa, close to both the values measured (not corrected) for the rehomogenized inclusion and the corrected values for the glassy inclusions.

The key question is then to understand whether the CO_2 present in the melt inclusions can be linked to the same source as the anatectic melt. The incorporation of carbon in slab-derived carbon-free silicate melt via the interaction between the latter and eclogite-facies metacarbonate rocks in collisional environment was documented in a migmatite system from the Sulu UHP terrane in China (*62*). However, in the Erzgebirge, such metacarbonate rocks are absent and there is evidence for internally derived crustal carbon being

carried in the slab during continental subduction in the vicinity of the Saidenbach eclogites. In some of these eclogites, where melt inclusions are notably absent, dolomite and calcite/aragonite were identified in both the matrix and as inclusions in garnet (*22*, *28*). In the adjacent quartzo-feldspathic granulites, carbonates are absent, but garnet contains carbon in the form of diamond as daughter phase in MSIs (interpreted as former fluids) and graphite is present as mineral inclusion in both garnet and zircon (*23*, *63*–*65*). While it is not yet possible to retrieve the stable carbon isotopic composition of rehomogenized melt inclusions and glassy inclusions of such a small size, isotopic data on bulk rock, graphite, and microdiamonds of the surrounding quartzo-feldspathic granulites and metasediments in general in the Erzgebirge do exist (*65*, *66*). Graphite and diamonds in inclusions in zircon and garnet in the quartzo-feldspathic granulites yield $\delta^{13}C$ values of −33 to −19 per mil (‰) and −29 to −17‰ (*65*, *67*), respectively, similar to that of bulk rock $\delta^{13}C$ values of the metasedimentary package of the Erzgebirge, −38 to −20‰ (Fig. 4B) (*68*, *69*). Such a strong organic signature in the Erzgebirge (*70*) indicates that neither mantle carbon (~−5‰) (*71*) nor sedimentary carbonates (−1 to +3‰) have played a substantial role in the carbon budget of this specific buried continental package (*70*). Carbon-rich siliciclastic Devonian sediments accumulated in passive margins have been suggested to be the source of this organic carbon (*65*). Taking into account that the protolith reacting with the metasomatic melt that originated Saidenbach eclogites was probably part of this original crustal package, and that the melt itself now trapped in the garnets originated in the same crustal package, we argue that the CO_2 content measured in rehomogenized melt inclusions share the same origin, i.e., organic. Moreover, this assumption is in agreement with experimental petrology works, suggesting that oxidative dissolution of graphite in oceanic metasediments is the main process controlling the production of CO_2 in the subducted sedimentary slab at depth >120 km (*72*).

Some of the surface carbon remains trapped in solid phases (i.e., diamond and graphite) in the subducted crust. The carbon-bearing melt phase is mobile and can thus escape the continental slab and metasomatize the overriding mantle as observed in the case of the melt in Saidenbach. As already discussed above, the partial melting of this metasomatized mantle wedge can originate hybrid melts, i.e., postcollisional (ultra)potassic magmas (*8*, *54*, *55*, *57*). The bulk mass of these hybrid magmas is provided by a mantle component (62 to 85%) contaminated by crustal material from the subducted slab [~10 to 20%; see (*54*)]. Assuming that partial melting of the mantle wedge occurs at depths similar to those of the eclogites studied here (130 to 150 km) and considering that the anatectic melt acted as a metasomatic agent, a simple mass balance calculation between our crustal melt (15 to 38%) and a primitive mantle melt (62 to 85%) composition [H_2O, 0.1 to 0.5 wt % (*73*); CO_2, 1800–2000 ppm (*74*)] suggests that the melt at the origin of postcollisional magmatism should contain 1.9 ± 0.7 wt % of H_2O and 8320 ± 4530 ppm of CO_2 (Fig. 4C). The compilation of the bulk volatiles content of (ultra)potassic postcollisional plutons (i.e., durbachites, shoshonites, and lamprophyres) from the Bohemian Massif indicates a similar average composition, 2.0 ± 0.6 wt % H_2O and 6130 ± 2490 ppm of CO_2. The H_2O concentration is also within error identical to the primitive melts of subduction zone basalts, 1.7 wt % H_2O (*73*). The isotopic composition of a mineral deposit associated with postcollisional plutons supports furthermore the hypothesis of organic carbon addition to the mantle, with $\delta^{13}C$ values in carbonates precipitating from magmatic fluids ranging from −16 to −3‰ (Fig. 4C) (*75*–*77*).

Although less widespread than oceanic subduction, continental subduction has the capacity to recycle and redistribute a substantial volume of volatiles and other incompatible trace elements first into the mantle and ultimately back to the overriding continental lithosphere, at least in part (Fig. 5). Such processes influence both the global growth and differentiation of the continental crust (*57*) and the long-term evolution of the carbon cycle. Our observations show that the endogenic carbon cycle is not limited to the consumption of the oceanic lithosphere alone and might then carry on after closure of the oceanic basin. The general scarcity of arc volcanism during continental subduction (*67*) suggests that buried volatiles are isolated from the surface cycle because they are stored within the lithospheric mantle wedge, the continental crust itself and in midcrustal, postcollisional plutons. The occurrence and preservation of such magmatic bodies in the geological records as far back as the Archean (*78*) favor the long-term solid storage of carbon at a time scale exceeding that of the Wilson cycle (i.e., rifting-subduction-collision). The recycling and reworking of the continental crust (*26*) constitutes a crucial aspect of the carbon cycle that extends beyond erosion and weathering (*26*). Future work aiming to reconstruct the carbon cycle in early Earth (e.g., preplate tectonics) will then need to integrate growth rate, differentiation, and evolution of the continental crust to understand how Earth achieved its current volatile exchange regime.

In conclusion, deeply subducted rocks of continental crust origin record fluid/melt-rock interaction processes taking place in the subarc depths. As continental crust material can be preserved over exceedingly long geological times, it is self-evident how these rocks are an excellent playfield for exploring ultradeep processes, which, despite being common during the subduction of the oceanic lithosphere, in the latter are often not preserved and thus not well constrained (*79*).

MATERIALS AND METHODS

Sample preparation

The investigation of the eclogites and the melt inclusions was performed on eight thin and double-polished thick sections (150 μm). The samples were initially studied with a polarized light optical microscope available at the University of Potsdam and melt inclusions were found in most of the garnet crystals of all sections investigated.

Microprobe and field-emission gun electron microprobe

The major element chemistry of the mineral phases and the glassy and rehomogenized melt inclusions were determined using a microprobe JEOL JXA-8200 available at the University of Potsdam. The analyses on glassy and rehomogenized inclusions were performed on inclusions exposed to the surface at 15 kV and 3.5 nA with a beam diameter of 1 μm. The calibration was performed using hydrous leucogranitic glass standards and the analytical conditions were kept constant on each session. The values of Na, K, Al, and Si were corrected to correct for alkali loss (*80*) with a factor determined using glass standards with similar H_2O content with respect to the glassy inclusions. A field-emission gun electron microprobe JEOL Hyperprobe JXA-8500F available at the Museum für Naturkunde in Berlin was used for the acquisitions of high-

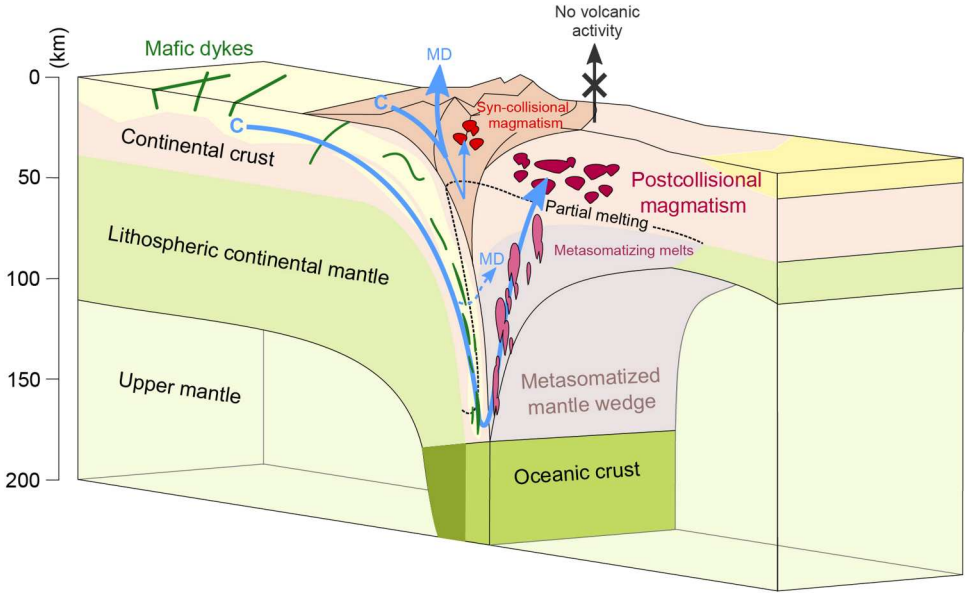

Fig. 5. Schematic diagram of the path of carbon (C) in continental subduction and collision. In collision zone, buried sedimentary carbon subject to Barrovian metamorphic conditions undergoes major metamorphic decarbonation (MD). A fraction of this carbon survives this process and is later remobilized during partial melting in the lower crust, eventually redistributed in syn-collisional granites (*26*). In the continental subduction zone, inorganic carbon would be more easily transferred to the mantle wedge during the early stage of subduction while organic carbon (C_{org}) would remain preferentially sequestered to the slab, allowing the transfer of organic matter to greater depths (*100*). In the case of the Saidenbach eclogites, C_{org} would be remobilized during partial melting to form a metasomatic agent, which, when interacting with the mantle wedge, would lead to the formation of hybrid melts and the genesis of (ultra)potassic postcollisional magmatic rocks.

resolution backscattered electron images and energy-dispersive spectrometer elemental mapping of mineral phases and melt inclusions.

Micro-Raman spectroscopy

The mineral assemblage inside the nanogranitoids and the nature of the glassy inclusions were determined using a HORIBA Jobin Yvon Confocal LabRAM HR 800 equipped with a Peltier-cooled multichannel CCD detector and an Olympus BX41 petrographic microscope. An air-cooled Nd-doped yttrium aluminum garnet (Nd:YAG) laser (λ = 532 nm, laser power on the sample was 2 to 3 mW) was used for excitation, and the spectra were acquired with an objective of 100×, a slit of 100 μm, and a confocal hole of 200 μm. All the analyses were performed with a grating of 300 lines/mm, doing three accumulations of 30 s in a range between 100 and 4000 cm^{-1} with a spectral resolution of 10 cm^{-1}.

Rehomogenization experiments

Nanogranitoid rehomogenization was performed at the condition expected for the formation of the garnet, 1000°C and 4.5 GPa. The experiment was conducted using a 1000-ton Walker-type multi-anvil module at the Earth Science Department "Ardito Desio" of the University of Milano. Inclusion-bearing garnets were mechanically removed from a double-polished thick section (~150 μm) and three garnet chips were loaded in a gold capsule separated by SiO_2 powder from each other and from the walls. The capsule was welded after being loaded. Cr-doped MgO octahedra of 25-mm edge length were used as pressure cells in 32-mm edge length tungsten carbide cubes. The assembly consisted of a ZrO_2 sleeve, a graphite heater, internal MgO spacers, and graphite end spacers ensuring electrical contact. Temperatures were controlled by an Eurotherm controller within ±2°C and measured by a Pt_{100}-$Pt_{90}Rh_{10}$ thermocouple (S type). Typical thermal gradients across the capsule are of about ±20°C. Pressure uncertainties were assumed ±3% according to the accuracy of calibrant reactions (*81*). The experimental sample was heated in 30 min and the temperature was kept at 1000°C for 24 hours.

Laser ablation inductively coupled plasma mass spectrometry analyses

Laser ablation inductively coupled plasma mass spectrometry (LA-ICP-MS) at the Department of Earth Science, ETH Zurich was used to determine the trace element content of mineral phases and melt inclusions. For the mineral phase, three thin sections were analyzed using a RESOlution (Australian Scientific Instruments/Applied Spectra) laser ablation system equipped with an S-155 dual-volume, fast-washout ablation cell (Laurin Technic, Australia). The analyses were performed with a laser repetition rate of 5 Hz with an on-sample energy of ~3.5 J/cm^2 and a spot size of 29 μm. For the melt inclusions investigation, 27 garnet chips were selected from three different double-polished thick sections. The laser ablation system used was the ETH-prototype GeoLas equipped with an Excimer ArF (193 nm) COMPex 102F laser source (Coherent, Germany). Sample chips were loaded in an in-house made, fully glassy, small-volume (ca. 6 cm^3) ablation cell. In this case, the laser repetition rate was 10 to 15 Hz with on-sample energy densities of 5 to 10 J/cm^2 and a variable spot size between 10 and 30 μm, depending on the size of the inclusion. The spot size was kept always slightly larger than the inclusion diameter to avoid unrepresentative sampling due to heterogeneity and to ensure complete ablation of the entire inclusion. For the same reason, our analyses targeted only melt inclusions below the sample surface and fully included in the

chip under observation. Both laser ablation systems are coupled with an Element XR (Thermo Fisher Scientific, Germany) sector-field ICP-MS. In both cases, the sample was transported to the ICP-MS through an aerosol made of He (5.0 grade) at ca. 0.5 to 1.1 liter min^{-1} flow to which was admixed make-up Ar gas (6.0 grade Ar) at ca. 1.0 liter min^{-1} before introduction into the plasma. The instrument was optimized for highest sensitivity on the high mass range, a low oxide production rate ($^{248}ThO^+/^{232}Th^+$ < 0.4%), and a U/Th ratio of ~1 on NIST SRM612 glass (ablated with 43-μm raster at 5 μm/s, 10 Hz, and 3.5 J/cm^2). A typical run consisted of ca. 30 s of gas blank acquisition followed by ablation, ca. 30 s for mineral analyses, and variable duration for inclusions, depending on their depth and size. Raw intensities were collected on low-resolution, triple-detector mode and peak jumping. The following isotopes were recorded (corresponding dwell times in milliseconds between parentheses): ^{7}Li (10), ^{11}B (10), ^{23}Na (10), ^{24}Mg (5), ^{27}Al (5), ^{29}Si (5), ^{31}P (10), ^{39}K (10), ^{43}Ca (5), ^{45}Sc (5), ^{49}Ti (10), ^{51}V (5), ^{53}Cr (5), ^{55}Mn (5), ^{57}Fe (5), ^{59}Co (5), ^{62}Ni (10), ^{63}Cu (10), ^{66}Zn (5), ^{85}Rb (10), ^{88}Sr (10), ^{89}Y (10), ^{90}Zr (25), ^{93}Nb (25), ^{133}Cs (10), ^{137}Ba (10), ^{139}La (50), ^{140}Ce (50), ^{141}Pr (50), ^{146}Nd (50), ^{147}Sm (25), ^{151}Eu (25), ^{157}Gd (25), ^{178}Hf (25), ^{181}Ta (25), ^{208}Pb (10), ^{232}Th (25), and ^{238}U (25). All data processing was performed offline using the software Signal Integration for Laboratory Laser Systems (SILLS) (*82*). The reference material used is NIST SRM612 for the minerals and NIST SRM610 for the melt inclusions (*83*). NIST SRM612 was measured with the same setup used for the mineral phases, whereas NIST SRM610 was measured with a repetition rate of 5 Hz, ca. 5 J/cm^{-1}, and a spot size of 30 μm in the case of inclusion analyses. The standard material was used to perform instrumental drift correction through conventional standard-sample bracketing and quantify trace element concentrations in both minerals and inclusions. In the case of inclusions, the contribution of the host matrix to the inclusion signal was deconvoluted as described in (*84*). For deconvolution and relative sensitivity correction, we used as internal standards the concentration of K_2O in the melt measured by electron microprobe (EMP) on preserved glassy inclusions and MgO as a host-dominated tracer owing to the large concentration contrast between garnet (ca. 7 wt %) and melt inclusions (ca. 0.20 wt %). The limit of the method used here is that elements strongly enriched in the host compared to the inclusions, such as HREE, Y, and some of the transition metals, are not quantifiable in the inclusions.

Nano-secondary ion mass spectrometry

To measure the content of H_2O and CO_2 in the melt inclusions, a CAMECA nano-secondary ion mass spectrometry (NanoSIMS) 50 installed at the Muséum National d'Histoire Naturelle of Paris was used following the procedure of Bartoli *et al.* (*18*) and Créon *et al.* (*85*). The analyses were performed on seven exposed preserved glassy inclusions on a thin section and one rehomogenized nano-granitoid mounted in indium in order to improve the vacuum (*86*), along with standard glasses. All samples and standards were gold-coated (20 nm thick). Before each analysis, the sample surface was presputtered using a Cs^+ primary beam (250 pA) over a surface area of 5 × 5 $μm^2$ for 2 min so that the coating was removed, surface contamination was avoided, and the sputtering steady-state regime was reached (*87*). Images of $^{28}Si^-$ and $^{56}Fe^{16}O^-$ secondary ions were used to identify the inclusions, and the analyses were performed with a 20-pA Cs + primary beam rastering a surface area of 3 × 3 $μm^2$. Each analysis is a stack of 200 cycles being 1.024 s long. Only the ions from the inner 1 × 1 $μm^2$ (use of beam blanking mode) were collected to minimize the surface contamination. Using electron multipliers with a dead time of 44 ns in multicollection mode, the secondary ions of $^{12}C^-$, $^{16}OH^-$ (proxy for H_2O), $^{19}F^-$, $^{28}Si^-$, and $^{56}Fe^{16}O^-$ were simultaneously collected. To resolve any mass interference on the selected ions, the mass resolving power was set to 5500. The analyses with unstable $^{16}OH^-/^{28}Si^-$ ratio were rejected. For H_2O calibration, three leucogranitic glasses were selected with known H_2O concentration varying between ~0.3 and 4.86 wt %: B H_2O = 300 ± 42 ppm, LGB1 H_2O = 4.9 wt %, and DL H_2O = 5.5 wt % (fig. S1) (*18*). For C correction, four trachyandesitic standards [STR 9, 10, 11, and 13; (*85*)] were used: part of shoshonitic lavas from Stromboli volcano experimentally doped in C and H_2O (*88*) and B. The analytical uncertainty on each measurement, based on counting statistics, was combined with the uncertainty on the calibration, based on confidence interval at 66%, by quadratic sum to obtain the 66% uncertainty.

CO_2 reintegration in primary glassy inclusions

To retrieve the total amount of CO_2 contained in glass inclusions, we reintegrated the concentration of CO_2, $[CO_2]_{vap}$ in parts per million, contained in the vapor bubble

$$[CO_2]vap = 10^6 \times \frac{\rho_{CO2} V_{vap}}{\rho_{melt} V_{melt}}$$

where V_{melt} and V_{vap} are the volume of the melt phase and the vapor bubble, respectively, and ρ_{melt} and ρ_{CO_2} are the density of the silicate melt and the density of the vapor bubble, respectively (*89*). The volume of the bubble and the inclusion are estimated using image analyses on three inclusions. At UHP conditions, a CO_2-rich vapor phase has a density ρ_{CO_2} of 1.04 ± 0.02 g cm^{-3} (*90*), and silicic melt, deduced from the modeling, has a density of ~2.75 ± 0.15 g cm^{-3}. The total CO_2 contents of the glassy inclusions is then obtained by summing the equivalent amount of CO_2 in the vapor bubble with the concentration of CO_2 measured in the melt phase by NanoSIMS. The average concentration of CO_2 in these inclusions is 20,177 ± 4444 ppm. As the vapor bubble is not visible in all the glassy inclusions due to removal of portion of the inclusion during polishing, we used the average value calculated above to correct from CO_2 concentration in the vapor phases in bubble-free inclusions.

LREE thermometry

LREE thermometry was applied to the data of this study based on the equation (*33*)

$$\ln \sum \mathrm{LREE} = 16.16\ (\pm 0.3) + 0.23\ (\pm 0.07)\sqrt{H_2O} - \frac{1149(\pm 410)}{T} - \frac{19.4(\pm 4)P}{T} + \ln X_{mnz}^{LREE}$$

where ln ∑ LREE is the sum of LREE concentration from La to Sm in the melt; for H_2O in the melt, we took the average value measured with NanoSIMS (3.89 wt %), P was 45 kbar, and for $\ln X_{mnz}^{LREE}$, we used the data from (*91*) (see table S8 for T values). It is worth noting that, although part of the same terrain, the monazite used for the calculation comes from a rock different from where the melt inclusions were identified. Therefore, because of the lack of

textural relationships, the temperature obtained estimates should be interpreted with caution.

Supplementary Materials

This PDF file includes:
Fig. S1
Tables S1 to S3
Tables S5 to S8

Other Supplementary Material for this manuscript includes the following:
Table S4

REFERENCES AND NOTES

1. M. L. Frezzotti, J. Selverstone, Z. D. Sharp, R. Compagnoni, Carbonate dissolution during subduction revealed by diamond-bearing rocks from the Alps. *Nat. Geosci.* **4**, 703–706 (2011).
2. E. M. Stewart, J. J. Ague, Pervasive subduction zone devolatilization recycles CO_2 into the forearc. *Nat. Commun.* **11**, 1–9 (2020).
3. A. Borghini, S. Ferrero, P. J. O'Brien, O. Laurent, C. Günter, M. A. Ziemann, Cryptic metasomatic agent measured in situ in Variscan mantle rocks: Melt inclusions in garnet of eclogite, Granulitgebirge, Germany. *J. Metamorph. Geol.* **38**, 207–234 (2020).
4. J. Hermann, Y. F. Zheng, D. Rubatto, Deep fluids in subducted continental crust. *Elements* **9**, 281–287 (2013).
5. C. J. Hawkesworth, A. I. S. Kemp, Evolution of the continental crust. *Nature* **443**, 811–817 (2006).
6. P. B. Kelemen, C. E. Manning, Reevaluating carbon fluxes in subduction zones, what goes down, mostly comes up. *Proc. Natl. Acad. Sci. U.S.A.* **112**, E3997–E4006 (2015).
7. S. F. Foley, G. Venturelli, D. H. Green, L. Toscani, The ultrapotassic rocks: Characteristics, classification, and constraints for petrogenetic models. *Earth Sci. Rev.* **24**, 81–134 (1987).
8. V. Janoušek, P. Hanžl, M. Svojtka, J. M. Hora, Y. V. E. Kochergina, P. Gadas, F. V. Holub, A. Gerdes, K. Verner, K. Hrdličková, J. S. Daly, D. Buriánek, Ultrapotassic magmatism in the heyday of the variscan orogeny: The story of the Třebíč Pluton, the largest durbachitic body in the Bohemian Massif. *Int. J. Earth Sci.* **109**, 1767–1810 (2020).
9. Y.-F. Zheng, J. Hermann, Geochemistry of continental subduction-zone fluids. *Earth Planets Sp.* **66**, 93 (2014).
10. D. Liu, Z. Zhao, D. C. Zhu, Y. Niu, D. J. DePaolo, T. M. Harrison, X. Mo, G. Dong, S. Zhou, C. Sun, Z. Zhang, J. Liu, Postcollisional potassic and ultrapotassic rocks in southern Tibet: Mantle and crustal origins in response to India-Asia collision and convergence. *Geochim. Cosmochim. Acta* **143**, 207–231 (2014).
11. T. Plank, C. E. Manning, Subducting carbon. *Nature* **574**, 343–352 (2019).
12. L. Q. Dai, K. Zhao, Z. F. Zhao, Y. F. Zheng, W. Fang, X. P. Zha, Y. J. An, Magnesium-carbon isotopes trace carbon recycling in continental subduction zone. *Lithos* **376–377**, 105774 (2020).
13. G. Nicoli, S. Ferrero, Nanorocks, volatiles and plate tectonics. *Geosci. Front.* **12**, 101188 (2021).
14. N. Malaspina, J. Hermann, M. Scambelluri, Fluid/mineral interaction in UHP garnet peridotite. *Lithos.* **107**, 38–52 (2009).
15. M. L. Frezzotti, S. Ferrando, The chemical behavior of fluids released during deep subduction based on fluid inclusions. *Am. Mineral.* **100**, 352–377 (2015).
16. P. J. Wallace, Volatiles in subduction zone magmas: Concentrations and fluxes based on melt inclusion and volcanic gas data. *J. Volcanol. Geotherm. Res.* **140**, 217–240 (2005).
17. H. Ni, H. Keppler, Carbon in silicate melts. *Rev. Mineral. Geochemistry.* **75**, 251–287 (2013).
18. O. Bartoli, B. Cesare, L. Remusat, A. Acosta-Vigil, S. Poli, The H_2O content of granite embryos. *Earth Planet. Sci. Lett.* **395**, 281–290 (2014).
19. S. Ferrero, J. J. Ague, P. J. O'Brien, B. Wunder, L. Remusat, M. A. Ziemann, J. Axler, High-pressure, halogen-bearing melt preserved in ultrahigh-temperature felsic granulites of the Central Maine terrane, Connecticut (U.S.A.). *Am. Mineral.* **106**, 1225–1236 (2021).
20. B. B. Carvalho, O. Bartoli, F. Ferri, B. Cesare, S. Ferrero, L. Remusat, L. S. Capizzi, S. Poli, Anatexis and fluid regime of the deep continental crust: New clues from melt and fluid inclusions in metapelitic migmatites from Ivrea Zone (NW Italy). *J. Metamorph. Geol.* **37**, 1–25 (2018).
21. S. Ferrero, R. J. Angel, Micropetrology: Are inclusions grains of truth? *J. Petrol.* **59**, 1671–1700 (2018).
22. P. J. O'Brien, M. A. Ziemann, Preservation of coesite in exhumed eclogite: Insights from Raman mapping. *Eur. J. Mineral.* **20**, 827–834 (2008).
23. B. Stöckhert, J. Duyster, C. Trepmann, H.-J. Massonne, Microdiamond daughter crystals precipitated from supercritical COH^+ silicate fluids included in garnet, Erzgebirge Germany. *Geology* **29**, 391–394 (2001).
24. H.-J. Massonne, in *Proceedings of the 7th int. Kimberlite Conf., Cape Town* (1999), pp. 552–554.
25. P. J. O'Brien, The fundamental Variscan problem: High-temperature metamorphism at different depths and high-pressure metamorphism at different temperatures. *Geol. Soc. London Spec. Publ.* **179**, 369–386 (2000).
26. G. Nicoli, A. Borghini, S. Ferrero, The carbon budget of crustal reworking during continental collision: Clues from nanorocks and fluid inclusions. *Chem. Geol.* **608**, 121025 (2022).
27. B. Cesare, A. Acosta-Vigil, O. Bartoli, S. Ferrero, What can we learn from melt inclusions in migmatites and granulites? *Lithos.* **239**, 186–216 (2015).
28. H.-J. J. Massonne, First find of coesite in the ultrahigh-pressure metamorphic area of the central Erzgebirge, Germany. *Eur. J. Mineral.* **13**, 565–570 (2001).
29. S. Ferrero, P. J. O'Brien, A. Borghini, B. Wunder, M. Wälle, C. Günter, M. A. Ziemann, A treasure chest full of nanogranitoids: An archive to investigate crustal melting in the Bohemian Massif. *Geol. Soc. London Spec. Publ.* **478**, 13–38 (2018).
30. S. Ferrero, M. A. Ziemann, R. J. Angel, P. J. O'Brien, B. Wunder, Kumdykolite, kokchetavite, and cristobalite crystallized in nanogranites from felsic granulites, Orlica-Snieznik Dome (Bohemian Massif): Not an evidence for ultrahigh-pressure conditions. *Contrib. Mineral. Petrol.* **171**, 1–12 (2016).
31. A. Borghini, S. Ferrero, B. Wunder, O. Laurent, P. J. O'Brien, M. A. Ziemann, Granitoid melt inclusions in orogenic peridotite and the origin of garnet clinopyroxenite. *Geology* **46**, 1007–1010 (2018).
32. K. H. Wedepohl, The composition of the continental crust. *Geochim. Cosmochim. Acta* **59**, 1217–1232 (1995).
33. A. S. Stepanov, J. Hermann, D. Rubatto, R. P. Rapp, Experimental study of monazite/melt partitioning with implications for the REE, Th and U geochemistry of crustal rocks. *Chem. Geol.* **300–301**, 200–220 (2012).
34. H.-J. Massonne, U. Grosch, P-T evolution of paleozoic garnet peridotites from the Saxonian Erzgebirge and the Aheim region, W.Norway. in *International Kimberlite Conference: Extended Abstracts* (1995), vol. 6, pp. 353–355.
35. L. J. Crisp, A. J. Berry, A new model for zircon saturation in silicate melts. *Contrib. Mineral. Petrol.* **177**, 71 (2022).
36. D. J. Rasmussen, T. A. Plank, P. J. Wallace, M. E. Newcombe, J. B. Lowenstern, Vapor-bubble growth in olivine-hosted melt inclusions. *Am. Mineral.* **105**, 1898–1919 (2020).
37. X. Y. Gao, Y. F. Zheng, Y. X. Chen, Dehydration melting of ultrahigh-pressure eclogite in the Dabie orogen: Evidence from multiphase solid inclusions in garnet. *J. Metam. Geol.* **30**, 193–212 (2012).
38. X. Y. Gao, Y. F. Zheng, Y. X. Chen, Z. Hu, Trace element composition of continentally subducted slab-derived melt: Insight from multiphase solid inclusions in ultrahigh-pressure eclogite in the Dabie orogen. *J. Metam. Geol.* **31**, 453–468 (2013).
39. X. Y. Gao, Y. F. Zheng, Y. X. Chen, Z. Hu, Composite carbonate and silicate multiphase solid inclusions in metamorphic garnet from ultrahigh-Peclogite in the Dabie orogen. *J. Metam. Geol.* **32**, 961–980 (2014).
40. Y. X. Chen, Y. F. Zheng, X. Y. Gao, Z. Hu, Multiphase solid inclusions in zoisite-bearing eclogite: Evidence for partial melting of ultrahigh-pressure metamorphic rocks during continental collision. *Lithos.* **200–201**, 1–21 (2014).
41. P. Liu, J. Zhang, H.-J. J. Massonne, Z. Jin, Polyphase solid-inclusions formed by interactions between infiltrating fluids and precursor minerals enclosed in garnet of UHP rocks from the Dabie Shan, China. *Am. Mineral.* **103**, 1663–1673 (2018).
42. N. Malaspina, J. Hermann, M. Scambelluri, R. Compagnoni, Polyphase inclusions in garnet-orthopyroxenite (Dabie Shan, China) as monitors for metasomatism and fluid-related trace element transfer in subduction zone peridotite. *Earth Planet. Sci. Lett.* **249**, 173–187 (2006).
43. S. Ferrando, M. L. Frezzotti, L. Dallai, R. Compagnoni, Multiphase solid inclusions in UHP rocks (Su-Lu, China): Remnants of supercritical silicate-rich aqueous fluids released during continental subduction. *Chem. Geol.* **223**, 68–81 (2005).
44. A. S. Stepanov, J. Hermann, D. Rubatto, A. V. Korsakov, L. V. Danyushevsky, Melting history of an ultrahigh-pressure paragneiss revealed by multiphase solid inclusions in garnet, Kokchetav massif Kazakhstan. *J. Petrol.* **57**, 1531–1554 (2016).
45. J. Hermann, C. J. Spandler, Sediment melts at sub-arc depths: An experimental study. *J. Petrol.* **49**, 717–740 (2008).
46. H.-J. Massonne, T. Fockenberg, Melting of metasedimentary rocks at ultrahigh pressure —Insights from experiments and thermodynamic calculations. *Lithosphere.* **4**, 269–285 (2012).

47. R. P. Rapp, E. B. Watson, C. F. Miller, Partial melting of amphibolite/eclogite and the origin of Archean trondhjemites and tonalites. *Precambrian Res.* **51**, 1–25 (1991).
48. G. Prouteau, B. Scaillet, M. Pichavant, Evidence for mantle metasomatism by hydrous silicic melts derived from subducted oceanic crust. *Nature* **410**, 197–200 (2001).
49. K. P. Skjerlie, A. E. Patiño Douce, The fluid-absent partial melting of a zoisite-bearing quartz eclogite from 1.0 to 3.2 GPa; implications for melting in thickened continetal crust and for subduction-zone processes. *J. Petrol.* **43**, 291–314 (2002).
50. R. P. Rapp, E. B. Watson, Dehydration melting of metabasalt at 8-32 kbar: Implications for continental growth and crust-mantle recycling. *J. Petrol.* **36**, 891–931 (1995).
51. A. Laurie, G. Stevens, Water-present eclogite melting to produce Earth's early felsic crust. *Chem. Geol.* **314–317**, 83–95 (2012).
52. L. G. Medaris, L. Ackerman, E. Jelínek, Z. D. Michels, V. Erban, J. Kotková, Depletion, cryptic metasomatism, and modal metasomatism (refertilization) of Variscan lithospheric mantle: Evidence from major elements, trace elements, and Sr-Nd-Os isotopes in a Saxothuringian garnet peridotite. *Lithos* **226**, 81–97 (2015).
53. L. Ackerman, E. Jelínek, L. G. Medaris, J. Ježek, W. Siebel, L. Strnad, Geochemistry of Fe-rich peridotites and associated pyroxenites from Horní Bory, Bohemian Massif: Insights into subduction-related melt-rock reactions. *Chem. Geol.* **259**, 152–167 (2009).
54. V. Janoušek, F. V. Holub, The causal link between HP-HT metamorphism and ultrapotassic magmatism in collisional orogens: Case study from the Moldanubian Zone of the Bohemian Massif. *Proc. Geol. Assoc.* **118**, 75–86 (2007).
55. J. F. Von Raumer, F. Finger, P. Veselá, G. M. Stampfli, Durbachites-Vaugnerites—A geodynamic marker in the central European Variscan orogen. *Terra Nov.* **26**, 85–95 (2014).
56. J. B. Murphy, Appinite suites: A record of the role of water in the genesis, transport, emplacement and crystallization of magma. *Earth Science Rev.* **119**, 35–59 (2013).
57. S. Couzinié, O. Laurent, J. F. Moyen, A. Zeh, P. Bouilhol, A. Villaros, Post-collisional magmatism: Crustal growth not identified by zircon Hf–O isotopes. *Earth Planet. Sci. Lett.* **456**, 182–195 (2016).
58. K. Schulmann, O. Lexa, V. Janoušek, J. M. Lardeaux, J. B. Edel, Anatomy of a diffuse cryptic suture zone: An example from the Bohemian Massif European variscides. *Geology* **42**, 275–278 (2014).
59. M. Gao, H. Xu, J. Zhang, S. F. Foley, Experimental interaction of granitic melt and peridotite at 1.5 GPa: Implications for the origin of post-collisional K-rich magmatism in continental subduction zones. *Lithos* **350–351**, 1–18 (2019).
60. T. Tacchetto, S. M. Reddy, O. Bartoli, W. D. A. Rickard, D. Fougerouse, D. W. Saxey, Z. Quadir, C. Clark, Pre-nucleation geochemical heterogeneity within glassy anatectic inclusions and the role of water in glass preservation. *Contrib. Mineral. Petrol.* **176**, 1–19 (2021).
61. O. Gianola, O. Bartoli, F. Ferri, A. Galli, S. Ferrero, L. S. Capizzi, C. Liebske, L. Remusat, S. Poli, B. Cesare, Anatectic melt inclusions in ultra high temperature granulites. *J. Metamorph. Geol.* **39**, 1–22 (2020).
62. S. Guo, J. Hermann, P. Tang, X. Chu, Y. Chen, B. Su, Formation of carbon-bearing silicate melts by melt-metacarbonate interaction at convergent plate margins. *Earth Planet. Sci. Lett.* **597**, 117816 (2022).
63. J. Schönig, H. von Eynatten, G. Meinhold, N. K. Lünsdorf, Diamond and coesite inclusions in detrital garnet of the Saxonian Erzgebirge Germany. *Geology* **47**, 715–718 (2019).
64. J. Schönig, H. von Eynatten, G. Meinhold, N. K. Lünsdorf, A. P. Willner, B. Schulz, Deep subduction of felsic rocks hosting UHP lenses in the central Saxonian Erzgebirge: Implications for UHP terrane exhumation". *Gondw. Res.* **87**, 320–329 (2020).
65. H. J. Massonne, W. Tu, δ13C signature of early graphite and subsequently formed microdiamond from the Saxonian Erzgebirge, Germany. *Terra Nov.* **19**, 476–480 (2007).
66. L. F. Dobrzhinetskaya, H. W. Green, N. Takahata, Y. Sano, K. Shirai, Crustal signature of $\delta^{13}C$ and nitrogen content in microdiamonds from Erzgebirge, Germany: Ion microprobe studies. *J. Earth Sci.* **21**, 623–634 (2010).
67. K. Wong, E. Mason, S. Brune, M. East, M. Edmonds, S. Zahirovic, Deep carbon cycling over the past 200 million years: A review of fluxes in different tectonic settings. *Front. Earth Sci.* **7**, 1–22 (2019).
68. W. Lorenz, Protolith analysis of metamorphic siliciclastic rocks in the Erzgebirge Mts Germany. *Sediment. Geol.* **97**, 43–67 (1995).
69. S. Triebold, H. von Eynatten, G. L. Luvizotto, T. Zack, Deducing source rock lithology from detrital rutile geochemistry: An example from the Erzgebirge, Germany. *Chem. Geol.* **244**, 421–436 (2007).
70. J. Krissansen-Totton, R. Buick, D. C. Catling, A statistical analysis of the carbon isotope record from the Archean to phanerozoic and implications for the rise of oxygen. *Am. J. Sci.* **315**, 275–316 (2015).
71. P. Deines, The carbon isotope geochemistry of mantle xenoliths. *Earth Sci. Rev.* **58**, 247–278 (2002).
72. S. Tumiati, S. Recchia, L. Remusat, C. Tiraboschi, D. A. Sverjensky, C. E. Manning, A. V. Brovarone, A. Boutier, D. Spanu, S. Poli, Subducted organic matter buffered by marine carbonate rules the carbon isotopic signature of arc emissions. *Nat. Commun.* **13**, 2909 (2022).
73. A. V. Sobolev, M. Chaussidon, H_2O concentrations in primary melts from supra-subduction zones and mid-ocean ridges: Implications for H_2O storage and recycling in the mantle. *Earth Planet. Sci. Lett.* **137**, 45–55 (1996).
74. A. Aiuppa, F. Casetta, M. Coltorti, V. Stagno, G. Tamburello, Melting in Earth' s upper mantle. *Nat. Geosci.* **14**, 697–703 (2021).
75. T. Wenzel, R. Oberhänsli, K. Mezger, K-rich plutonic rocks and lamprophyres from the Meissen Massif (northern Bohemian Massif): Geochemical evidence for variably enriched lithospheric mantle sources. *Neues Jahrb. fur Mineral. Abhandlungen.* **175**, 249–293 (2000).
76. K. Malý, Z. Dolníček, Pb-Zn-Ag vein mineralization of the central part of the Českomoravská vrchovina Upland (Czech Republic): S, C, and O stable isotope study. *Bull. Geosci.* **80**, 307–319 (2005).
77. J. Zachariáš, K. Žák, M. Pudilová, L. W. Snee, Multiple fluid sources/pathways and severe thermal gradients during formation of the Jílové orogenic gold deposit, Bohemian Massif, Czech Republic. *Ore Geol. Rev.* **54**, 81–109 (2013).
78. S. Couzinié, J.-F. Moyen, A. Villaros, J.-L. Paquette, J. H. Scarrow, C. Marignac, Temporal relationships between Mg-K mafic magmatism and catastrophic melting of the Variscan crust in the southern part of Valay Complex (Massif Central France). *J. Geosci.* **59**, 69–86 (2014).
79. J. Hermann, D. Rubatto, *Subduction of Continental Crust to Mantle Depth: Geochemistry of Ultrahigh-Pressure Rocks* (2013), vol. 4.
80. G. B. Morgan, D. London, Effect of current density on the electron microprobe analysis of alkali aluminosilicate glasses. *Am. Mineral.* **90**, 1131–1138 (2005).
81. P. Fumagalli, S. Poli, Experimentally determined phase relations in hydrous peridotites to 6.5 GPa and their consequences on the dynamics of subduction zones. *J. Petrol.* **46**, 555–578 (2005).
82. M. Guillong, D. L. Meier, M. M. Allan, C. A. Heinrich, B. W. D. Yardley, SILLS: A Matlab-based program for the reduction of laser ablation ICP–MS data of homogeneous materials and inclusions. *Mineral. Assoc. Canada Short Course.* **40**, 328–333 (2008).
83. K. P. Jochum, U. Weis, B. Stoll, D. Kuzmin, Q. Yang, I. Raczek, D. E. Jacob, A. Stracke, K. Birbaum, D. A. Frick, D. Günther, J. Enzweiler, Determination of reference values for NIST SRM 610–617 glasses following ISO guidelines. 35, 397–429 (2011).
84. W. E. Halter, T. Pettke, C. A. Heinrich, B. Rothenrutishauser, B. Rothen-rutishauser, Major to trace element analysis of melt inclusions by laser-ablation ICP-MS: Methods of quantification. *Chem. Geol.* **183**, 63–86 (2002).
85. L. Créon, G. Levresse, L. Remusat, H. Bureau, G. Carrasco-Núñez, New method for initial composition determination of crystallized silicate melt inclusions. *Chem. Geol.* **483**, 162–173 (2018).
86. C. Aubaud, A. C. Withers, M. M. Hirschmann, Y. Guan, L. A. Leshin, S. J. Mackwell, D. R. Bell, Intercalibration of FTIR and SIMS for hydrogen measurements in glasses and nominally anhydrous minerals. *Am. Mineral.* **92**, 811–828 (2007).
87. A. Thomen, F. Robert, L. Remusat, Determination of the nitrogen abundance in organic materials by NanoSIMS quantitative imaging. *J. Anal. At. Spectrom* **29**, 512–519 (2014).
88. H. Bureau, P. Trocellier, C. Shaw, H. Khodja, N. Bolfan-Casanova, S. Demouchy, Determination of the concentration of water dissolved in glasses and minerals using nuclear microprobe. *Nucl. Instruments Methods Phys. Res. Sect. B Beam Interact. with Mater. Atoms.* **210**, 449–454 (2003).
89. P. E. Wieser, H. Lamadrid, J. Maclennan, M. Edmonds, S. Matthews, K. Iacovino, F. E. Jenner, C. Gansecki, F. Trusdell, R. L. Lee, E. Ilyinskaya, Reconstructing magma storage depths for the 2018 Ki?lauean eruption from melt inclusion CO_2 contents: The importance of vapor bubbles. *Geochemistry Geophys. Geosystems.* **22**, 1–30 (2021).
90. M. Berkesi, K. Hidas, T. Guzmics, J. Dubessy, R. J. Bodnar, C. Szabó, B. Vajna, T. Tsunogae, Detection of small amounts of H_2O in CO_2-rich fluid inclusions using Raman spectroscopy. *J. Raman Spectrosc.* **40**, 1461–1463 (2009).
91. H.-J. Massonne, A. Kennedy, L. Nasdala, T. Theye, Dating of zircon and monazite from diamondiferous quartzofeldspathic rocks of the Saxonian Erzgebirge—Hints at burial and exhumation velocities. *Mineral. Mag.* **71**, 407–425 (2007).
92. O. Bartoli, A. Acosta-Vigil, S. Ferrero, B. Cesare, Granitoid magmas preserved as melt inclusions in high-grade metamorphic rock. *Am. Mineral.* **101**, 1543–1559 (2016).
93. S.-S. Sun, W. F. McDonough, Chemical and isotopic systematics of oceanic basalts: Implications for mantle composition and processes. *Geol. Soc. London Spec. Publ.* **42**, 313–345 (1989).
94. W. F. McDonough, S.-S. Sun, W. F. Mcdonough, S.-S. Sun, W. F. McDonough, S.-S. Sun, The composition of the Earth. *Chem. Geol.* **120**, 223–253 (1995).
95. M. Němec, J. Zachariáš, The Krásná Hora, Milešov, and Příčovy Sb-Au ore deposits, Bohemian Massif: Mineralogy, fluid inclusions, and stable isotope constraints on the deposit formation. *Miner. Depos.* **53**, 225–244 (2018).

96. J. M. Hora, A. S. Tabaud, V. Janoušek, Y. V. Erban Kochergina, Potassic magmas of the Vosges Mts. (NE France) delimit the areal extent and nature of long-gone Variscan orogenic mantle domains. *Lithos* **402–403**, 106304 (2021).
97. F. V. Holub, Petrology of inclusions as a key to petrogenesis of the durbachitic rocks from Czechoslovakia. *TMPM Tschermaks Mineral. und Petrogr. Mitteilungen.* **24**, 133–150 (1977).
98. D. R. Bowes, J. Košler, Geochemical comparison of the subvolcanic appinite suite of the British Caledonides and the durbachite suite of the Central European Hercynides: Evidence for associated shoshonitic and Granitic Magmatism. *Mineral. Petrol.* **48**, 47–63 (1993).
99. O. Shrbený, V. Macháček, Microelements in melilitic rocks of Northern Bohemia. *Čas. Pro miner. Geol.* **19**, 15–25 (1974).
100. P. Bouilhol, B. Debret, E. Inglis, K. W. Burton, M. Warembourg, T. Grocolas, T. Rigaudier, J. Villeneuve, Decoupling of inorganic and organic carbon during slab mantle devolatilisation. *Nat. Commun.* **13**, 308 (2022).

Acknowledgments: We thank L. Hecht, F. Kaufmann, and C. Günter for help during the analyses and C. Fischer for sample preparation. **Funding:** We thank the German Federal Ministry for Education and Research and the Deutsche Forschungsgemeinschaft (projects FE 1527/2-1, FE 1527/2-2, and FE 1527/4-1 to S.F.) and the Alexander von Humboldt Foundation (funding to G.N.). We are grateful to V. Janoušek for discussions over the years, to J. Hermann and an anonymous reviewer for the insightful comments, and to G. Gaetani for the editorial handling. **Author contributions:** A.B., S.F., and P.J.O. designed the project; P.J.O. collected the samples; and A.B. conducted the petrographic study with the help of S.F. A.B. performed all the analyses with the collaboration of O.L. for the trace elements data, L.R. for the volatiles data, and G.B. and S.M. for the rehomogenization experiments. G.N. corrected the glass inclusion analyses values for volatiles and performed the phase equilibria modeling. A.B. and G.N. designed the artwork with the collaboration of S.F. All authors participated in extensive discussions on data evaluation, interpretation, and preparation of the manuscript. **Competing interests:** The authors declare that they have no competing interests. **Data and materials availability:** All data needed to evaluate the conclusions in the paper are present in the paper and/or the Supplementary Materials.

Submitted 8 March 2022
Accepted 10 January 2023
Published 10 February 2023
10.1126/sciadv.abp9482